HHS Public Access

Author manuscript

Annu Rev Neurosci. Author manuscript; available in PMC 2019 March 27.

Published in final edited form as:

Annu Rev Neurosci. 2016 July 08; 39: 385–407. doi:10.1146/annurev-neuro-070815-014045.

Maps of the Auditory Cortex

Alyssa A. Brewer and **Brian Barton**

Department of Cognitive Sciences and Center for Hearing Research, University of California, Irvine, California 92697; aabrewer@uci.edu, bbarton@uci.edu

Abstract

One of the fundamental properties of the mammalian brain is that sensory regions of cortex are formed of multiple, functionally specialized cortical field maps (CFMs). Each CFM comprises two orthogonal topographical representations, reflecting two essential aspects of sensory space. In auditory cortex, auditory field maps (AFMs) are defined by the combination of tonotopic gradients, representing the spectral aspects of sound (i.e., tones), with orthogonal periodotopic gradients, representing the temporal aspects of sound (i.e., period or temporal envelope). Converging evidence from cytoar-chitectural and neuroimaging measurements underlies the definition of 11 AFMs across core and belt regions of human auditory cortex, with likely homology to those of macaque. On a macrostructural level, AFMs are grouped into cloverleaf clusters, an organizational structure also seen in visual cortex. Future research can now use these AFMs to investigate specific stages of auditory processing, key for understanding behaviors such as speech perception and multimodal sensory integration.

Keywords

auditory field maps; tonotopy; periodotopy; cortical mapping; phase-encoded fMRI

INTRODUCTION

Auditory processing in humans is crucial for a variety of our sensory experiences, including orienting and responding to environmental sounds, enjoying music, and communicating through speech. Although much attention over the past few decades has been devoted to auditory behavior with psychoacoustics research and to higher-level audition with research into speech production and comprehension, investigations into the structure and function of lower-level cortical processing have been relatively limited, especially in human cortex. However, an understanding of the organization of primary and lower-level auditory cortex is key for understanding both the neural underpinnings of auditory behavior and the inputs into speech processing networks.

DISCLOSURE STATEMENT

The authors are not aware of any affiliations, memberships, funding, or financial holdings that might be perceived as affecting the objectivity of this review.

Inputs to Auditory Cortex

Auditory processing begins in the ear, where hair cells along the basilar membrane of the human cochlea in the inner ear respond to sound frequencies (i.e., tones) topographically, with frequency selectivity running smoothly along the membrane from high at one end to low at the other. This tonotopic (or cochleotopic) organization is preserved as auditory information is processed and passed on from the inner ear through the brainstem (i.e., from cochlear nucleus to superior olive to medial lemniscus to inferior colliculus) to the medial geniculate nucleus (MGN) of the thalamus and into primary auditory cortex (PAC; for additional discussion, see Kaas & Hackett 2000, Saenz & Langers 2014). PAC is located along the superior temporal gyrus (STG) in macaque monkey and along Heschl's gyrus (HG), running from STG into the lateral sulcus (LS), in human (Figures 1 and 2).

The preservation of tonotopic organization, one dimension of acoustic feature space, from the basilar membrane to auditory cortex allows for a common reference frame in this hierarchically organized sensory system (Kaas 1997, Wessinger et al. 2001). Such a reference frame is mirrored in the organization of the visual system, which preserves the retinal organization throughout the hierarchical visual processing in cortex (Brewer & Barton 2012, Wandell & Winawer 2010, Wandell et al. 2007). The visual system topography centers on repeating gradient representations of two orthogonal dimensions of visual space, eccentricity and polar angle, which combine to form sensory cortical field maps (CFMs). These multiple, distinct, and complete representations of visual space known as visual field maps (VFMs) are currently measured routinely in visual cortex (e.g., Brewer & Barton 2012; DeYoe et al. 1996; Engel et al. 1994, 1997; Sereno et al. 1995; Wandell et al. 2007). Recent findings have also demonstrated repeating gradient representations of two orthogonal dimensions of acoustic feature space around PAC: tonotopy, or maps of the spectral components of sound, and periodotopy, or maps of the temporal components of sound (Barton et al. 2012, Baumann et al. 2015, Herdener et al. 2013, Langner et al. 1997). These orthogonal gradients similarly form CFMs in the auditory system called auditory field maps (AFMs).

The Cortical Field Map: A Key Functional Architecture in Sensory Cortex

The CFM is one of the more important, larger-scale, organizing principles of sensory cortical organization, in which neurons whose sensory receptive fields are positioned next to one another in sensory feature space are located next to one another in cortex. This topographic organization of CFMs is thought to allow for efficient connectivity among neurons that represent nearby aspects in sensory feature space, likely necessary for such processes as lateral inhibition and to compactly organize neural signals ranging from the molecular level to that of the cerebral hemisphere (Chklovskii & Koulakov 2004, Mitchison 1991, Moradi & Heeger 2009, Shapley et al. 2007). Although the term map has often been applied nonspecifically to topographical gradients or other similar cortical representations, it is useful in the study of sensory processing to explicitly define a CFM according to very precise criteria: (*a*) A CFM is composed of two (or more) orthogonal, nonrepeating topographical representations of fundamental sensory dimensions; (b) each of these topographical representations must be organized as a generally contiguous, orderly gradient; (*c*) each CFM should represent a substantial portion of sensory space; and (*d*) the general

features of each CFM should be consistent across individuals (Supplemental Figures 1–4; Barton et al. 2012, Baumann et al. 2011, Brewer & Barton 2012, Brewer et al. 2005, DeYoe et al. 1996, Press et al. 2001, Sereno et al. 1995, Van Essen 2003, Wandell et al. 2007, Zeki 2003). For additional discussion and a brief primer on cortical field mapping, follow the Supplemental Materials link in the online version of this article or at http://www.annualreviews.org/.

As we discuss further below, this specific CFM definition provides an in vivo measurement that can localize the distinct borders of a particular cortical region across individuals reliably, despite the high degree of cortical variability across subjects (Amunts et al. 1999; Clarke & Morosan 2012; Dougherty et al. 2003; Leonard et al. 1998; Rademacher et al. 1993, 2001). In contrast, the measurement of a single topographical gradient (e.g., tonotopy), which represents only one aspect of the organization of the peripheral sensing organ (e.g., frequency along the basilar membrane of the cochlea), does not allow for the definition of these borders. Topographical gradients of a single sensory dimension suggest that one or more CFMs are present, but there is no way to divide up these representations accurately into specific CFMs without measurements of a second overlapping and orthogonal dimension (Brewer & Barton 2012, Wandell et al. 2007). A single gradient across a region of sensory cortex may correspond to one CFM or to many (Supplemental Figure 4). Similarly, measurements of two overlapping gradients that are parallel rather than orthogonal will not provide a measurement that maps all the points in sensory space uniquely. For example, a region of visual cortex with parallel eccentricity and polar angle gradients would represent a narrow spiral of visual space rather than the entire visual field (Brewer & Barton 2012, Brewer et al. 2005, Wade et al. 2002). Furthermore, the definition of a CFM is also distinguished from that of a cortical area, the definition of which relies not only on topographical measurements but also on measures of function, cytoarchitecture, and connectivity, which can produce conflicting data (for additional discussion, see Supplemental Materials Text; Brewer & Barton 2012, Van Essen 2003, Wandell et al. 2007, Zeki 2003).

The Significance and Utility of Cortical Field Maps

CFMs are currently being studied in the visual, somatosensory, and auditory systems of many species (e.g., Barton et al. 2012, Kaas 1997, Sanchez-Panchuelo et al. 2010, Wandell et al. 2005). Each CFM is expected to subserve a specific computation or set of computations that underlie particular perceptual behaviors by facilitating the comparison and combination of the information carried by the various specialized neuronal populations within this cortical region (Brewer & Barton 2012, Chklovskii & Koulakov 2004, Wandell et al. 2007, Zeki & Bartels 1999). These computations may underlie relatively general sensory processing, as seen in primary sensory cortex (e.g., V1 or PAC), or may relate to more specific higher-order perceptual processing [e.g., specialized visual motion processing in the medial temporal visual area (MT)], with these computations typically becoming more complex as the neural processing continues up through the sensory hierarchy (Van Essen 2003).

Measuring CFMs in vivo allows for the systematic exploration of computations across a particular sensory cortex; thus, the definition and characterization of CFMs have been indispensable in the investigation of the structure and function of human cortex. Measuring the organization of individual CFMs helps elucidate the stages of distinct sensory processing pathways and can be used to track how the cortex changes under various disorders. Furthermore, CFMs serve as excellent and dependable independent localizers for investigations of particular functions across individuals. The accurate determination of CFM boundary organization is therefore also vital to this investigation, or the region of cortex specifically devoted to a particular computation—i.e., one CFM—will not be isolated or localized correctly (Brewer & Barton 2012).

CYTOARCHITECTURE IN AUDITORY CORTEX

It is valuable when determining the organization of CFMs to consider related research on structural differences across cortex, including findings drawn from postmortem anatomical dissection, laminar staining techniques, and tracer studies of anatomical connectivity. Converging evidence from these other sources can lend support to a particular set of definitions for CFM boundaries when all measures agree (for additional discussion, see Supplemental Materials Text). In some cases, however, CFM borders do not match the borders defined by these measurements exactly, likely owing to differences in measurement noise and resolution and to the possibility of multiple CFMs—multiple computational regions—existing within a single cytoarchitectural region, as is seen in extrastriate visual cortex beyond primary visual cortex (Wandell et al. 2005). The extrastriate region in occipital cortex, for example, contains well over 10 VFMs, but most are contained within just two cytoarchitectural regions: Brodmann areas 18 and 19 (Amunts et al. 2000, Brewer & Barton 2012). Even so, examining measurements from cytoarchitecture and connectivity studies is a very useful starting point for developing expectations for CFM organization, especially when conducting studies in a relatively new field such as auditory field mapping.

Structural Features in Macaque Auditory Cortex

Cytoarchitectural measurements in macaque have been a primary aspect of the development of our understanding of the organization of human auditory cortex. Two models of macaque auditory cortex that are particularly useful for comparison to human are described in Figure 3. For each comparative study presented here, we have developed an approximate model of the results of the measurements by taking into account the individual data, group-averaged data, or both (depending on availability in the study) as well as any information presented regarding the size and location of the specific measures. In the combined measurements of Pandya & Sanides (1973) and Galaburda & Pandya (1983), several main cytoarchitectural regions have been delineated spanning cortex from STG to the circular sulcus (CiS) within LS (Figure 3d). A central strip of regions contains, from posterior to anterior, the caudal parakoniocortical area (PaAc), koniocortical area (KA), and rostral parakoniocortical area (PaAr). Just medial to this strip toward CiS are the retroinsular temporal area (reIt), prokoniocortical area (ProA), and parainsular area (PaI). Three more areas lie just lateral to the central strip and overlap STG: the temporoparietal area (Tpt), lateral parakoniocortical area (PaAlt), and temporalis superior 3 (Ts3, also called rostral superior temporal area 3).

Since these measurements were taken, additional cytoarchitectural and connectivity studies have further subdivided and renamed these regions and paired them to functional measurements from electrophysiology and functional magnetic resonance imaging (fMRI). Prominent among these are studies with converging evidence for 13 auditory cortical areas grouped into core, medial belt, lateral belt, and parabelt regions, with primary, secondary, and tertiary levels of processing, respectively (Kaas & Hackett 2000; for additional discussion of the differences between CFMs and cortical areas, see Supplemental Materials Text). Figure 3c illustrates this organization overlaid with tonotopic measurements. The concept of a multiarea core as PAC, rather than a single area such as V1 as seen in visual cortex, can generally be ascribed to measurements across all three core areas demonstrating the dense thalamic inputs from MGN; the expanded layer IV; and the high expression of cytochrome oxidase, acetylcholinesterase, and parvalbumin characteristic of primary sensory cortices (Galaburda & Pandya 1983, Hackett 2011, Hackett et al. 1998a, Jones et al. 1995, Kaas & Hackett 2000, Merzenich & Brugge 1973, Molinari et al. 1995, Morel et al. 1993). The naming scheme for the auditory areas in macaque arises from their axis of orientation in the macaque brain, where areas are named with respect to the first auditory area, A1. A1 lies in the caudal portion of the core, with the successively more rostral portions named as the rostral area (R) and the rostral temporal area (RT). These core regions likely correspond to the Pandya-Sanides-Galaburda model, with A1 and R together homologous to KA. The slightly differently staining RT then would correspond to the separate area of PaAr (compare common colors between Figure 3c,d).

The anatomical naming scheme has been adopted for the other areas as well, with four medial and four lateral areas in the belt, encircling the core. The medial belt likely corresponds to the Pandya-Sanides-Galaburda model as follows: rostral temporal medial area (RTM) to PaI, rostral medial area (RM) to ProA, medial medial area (MM) to ProA or reIt, and caudal medial area (CM) to reIt or PaAc (de la Mothe et al. 2006, Galaburda & Pandya 1983, Hackett et al. 1998 a, Morel et al. 1993, Pandya & Sanides 1973, Tian & Rauschecker 2004). Similarly, the lateral belt likely corresponds to the Pandya-Sanides-Galaburda model as follows: rostral temporal lateral area (RTL) to Ts3, anterior lateral area (AL) and medial lateral area (ML) to the medial portions of lateral parakoniocortical area (PaAlt) and Tpt, and caudal lateral area (CL) to part of caudal parakoniocortical area (PaAc; Galaburda & Pandya 1983, Hackett et al. 1998a, Moerel et al. 2014, Morel et al. 1993, Pandya & Sanides 1973, Rauschecker & Tian 2004, Rauschecker et al. 1995). Outside of that, several additional areas have been proposed to form caudal and rostral parabelt (CPB and RPB) regions, derived from the lateral sections of Tpt, PaAlt, and Ts3 along STG (Galaburda & Pandya 1983; Hackett et al. 1998a,b; Pandya & Sanides 1973; Romanski et al. 1999). These cytoarchitectural divisions have paved the way for functional studies of topography in auditory cortex and for comparison to human cortex.

Structural Features in Human Auditory Cortex

Similar, yet not identical, cytoarchitectural features in human indicate that, during the approximately 25 million years of evolutionary separation between the species (Hedges & Kumar 2003, Krubitzer & Seelke 2012), the auditory core, belt, and parabelt have rotated medially from macaque STG onto a new region within LS in human called HG (Figures 1

and 2; Supplemental Figure 6). This region can exist in humans as a single gyrus or as double gyri, with the core and belt usually either mostly centered on the single HG or overlapping both gyri in the case of two (Amunts et al. 1999, Leonard et al. 1998, Morosan et al. 2001).

Current research into the cytoarchitecture of human auditory cortex arose from the pioneering studies of von Economo & Koskinas (1925). Since that time, studies using similar staining techniques as those that identified macaque core have mostly converged to reveal a similar pattern of darkly staining cells on HG, surrounded by cells that stain similarly to macaque belt (Fullerton & Pandya 2007, Galaburda & Sanides 1980, Hackett et al. 2001, Rivier & Clarke 1997, Sweet et al. 2005). These data also suggest that the human analogue to CM is located on the medial wall of LS, between the tip of HG and the circular gyrus. These measurements thus anchor the expected orientation of CFMs from a strictly rostral-caudal axis for A1 to R to RT, as in macaque monkey along STG, to a medial-lateral axis in human along HG.

Figure 3f,g shows two popular models of human cytoarchitecture that have general similarities. Galaburda & Sanides (1980) with Fullerton & Pandya (2007) describe the medial koniocortical area (KAm), the lateral koniocortical area (KAlt), and PaAr along HG, which likely correspond to human core areas hA1, hR, and hRT (h added for human), respectively, and to macaque areas KA and PaAr, with KAm and KAlt as medial and lateral subdivisions of KA (but note that macaque is subdivided similarly in some versions of the Pandya-Sanides-Galaburda model; Figure 3f,d). Medial belt is composed of ProA, likely corresponding to macaque PaI, ProA and possibly reIt. hCM and hCL are generally grouped with the medial and lateral belts but differ in cytoarchitecture as caudal-dorsal parakoniocortical area (PaAc/d), likely corresponding to macaque PaAc. Lateral belt is likely composed of lateral parakoniocortical area, internal (PaAi), corresponding to the medial aspect of macaque PaAlt, and a parabelt region surrounds the posterior-lateral edge of this as lateral parakoniocortical area, external (PaAe), likely corresponding to the lateral aspect of macaque PaAlt on the STG (Kaas & Hackett 2000). Posterior to parabelt PaAe is Tpt in the planum temporale (Figure 2), likely corresponding to at least the posterior part of the same region in macaque.

A more recently developed model by Morosan et al. (Clarke & Morosan 2012, Morosan et al. 2001) defines differently named regions (Figure 3g), but the organization has a strong correlation to that in Figure 3f described above. A three-area core lies along HG, with Te1.1, Te1.0, and Te1.2 likely corresponding to hA1, hR, and hRT (also KAm, KAlt, and PaAr), respectively. Part of the medial belt likely corresponds to TI1, and part of the lateral belt likely corresponds to Te2.1. A homologue to the parabelt may exist in the posterior-lateral two regions, Te2.2 and Te3. Although these cytoarchitectural regions may not always correspond directly to CFM borders, they definitely define a scale and general position that can be used to verify functional topographical measurements. In other words, we should expect CFM measurements to define core as three regions of this approximate size running from hA1 at the tip of HG to hRT at the base along STG.

TONOTOPY: THE FIRST DIMENSION OF AUDITORY FIELD MAPS

To identify tonotopic gradients in cortex, researchers typically present an array of pure tones, tone complexes, or narrowband noise using a set of stimuli that activate most or all of the topographic regions of interest in auditory cortex (e.g., Barton et al. 2012, Humphries et al. 2010, Merzenich & Brugge 1973, Petkov et al. 2006, Talavage et al. 2004, Woods et al. 2010; for additional discussion of cortical field mapping techniques, see Supplemental Materials Text and Supplemental Figure 1). For clarity, this section discusses studies that measured only tonotopic gradients; the few studies that measured both tonotopic and periodotopic gradients, and thus measured AFMs, are discussed later under the section entitled Periodotopy: The Second Dimension of Auditory Field Maps.

Tonotopic Organization in the Monkey Auditory System

The tonotopic representations in macaque cortex have been delineated using a range of techniques, from single-and multiunit electrode recordings (Kosaki et al. 1997, Kusmierek & Rauschecker 2009, Merzenich & Brugge 1973, Morel et al. 1993) to parvalbumin immunoreactivity staining (Kosaki et al. 1997) to fMRI topographic measurements (Joly et al. 2014; Petkov et al. 2006, 2009; Tanji et al. 2010). Until only very recently, such studies have had to deal with issues in determining how to divide up the tonotopic gradients into separate regions without the measurement of a second, orthogonal topography. However, in nonhuman primates, researchers have had the opportunity to use electrophysiology in conjunction with cytoarchitectural fields in the same monkey. Thus, these measures of tonotopic gradients can be compared directly to cytoarchitectural fields (Kosaki et al. 1997, Kusmierek & Rauschecker 2009, Merzenich & Brugge 1973, Morel et al. 1993) and/or to other functional differences observed among core, medial belt, and lateral belt, such as bandwidth selectivity (e.g., Kusmierek & Rauschecker 2009, Rauschecker & Tian 2004, Rauschecker et al. 1995, Recanzone et al. 2000, Tian & Rauschecker 2004). Such combined measurements allow the studies to determine cortical area divisions within the tonotopic gradients, although in some cases the boundaries of topography will not match those of cytoarchitecture perfectly, as described above (for additional discussion, see Supplemental Materials Text).

fMRI studies in macaque do not typically correlate the functional tonotopic measurements specifically with electrophysiological or cytoarchitectonic investigations in the same animals owing to the difficulty of using the combination of techniques in one subject. However, most macaque fMRI studies prior to the orthogonal measurement of periodicity have dealt with this issue by including measurements in the same monkey of general differences in other properties between core and belt. Combining fMRI tonotopy with other fMRI measures such as bandwidth selectivity (Petkov et al. 2006) and structural measures such as cortical myelination (Joly et al. 2014) allows for at least an estimate of the core/belt border, although belt/parabelt differences in these measures have not been as clear.

These measurements of macaque tonotopic responses have generally supported and been integrated into the organization of core, belt, and parabelt defined by cytoarchitectural methods (Figure 3a,c; for additional discussion, see Kaas & Hackett 2000, Kajikawa et al. 2015). The majority of the studies demonstrate strongly that the three core areas are divided

by reversals in the tonotopic representations, with one full gradient in each area. These gradients are oriented in a high-to-low-to-high-to-low pattern of frequency representations, with high tones represented in the broadly caudal aspect of A1 and low tones in the broadly rostral aspect that reverses into R. RT then mirrors R, with R's rostral border in a high region reversing through RT back to a low representation. These tonotopic gradients roughly extend medially and laterally from core to form the gradient reversals of the belt regions in line with each of the core reversals, although these measurements tend to be less clear in many studies. An additional low representation exists posterior to A1 and comprises the posterior boundaries of CM and CL. Finally, a recent electro-physiological study that is the first to analyze specifically the tonotopic organization of the parabelt suggests that the tonotopic gradients of core and belt continue laterally in parallel to demark the boundaries of the parabelt caudal and rostral subdivisions, with a low-frequency gradient reversal at the boundary of CPB and RPB bounded by high-frequency representations on each side (Kajikawa et al. 2015).

Tonotopic Organization in the Human Auditory System

In contrast to macaque, human measurements of tonotopic organization have been complicated more severely by the lack of a measurement of a second, orthogonal dimension to mark the boundaries accurately among cortical areas in core, belt, and parabelt. The tonotopic gradient data presented in these studies are actually quite similar, but the models of core and belt organization put forth based on the interpretation of the data vary widely, with differences arising for many reasons (Figure 4; e.g., Da Costa et al. 2011; Dick et al. 2012; Formisano et al. 2003; Humphries et al. 2010; Moerel et al. 2012,2014; Talavage et al. 2004; Thomas et al. 2015; Upadhyay et al. 2007; Woods et al. 2010). First, human fMRI studies have differed greatly in the level of attention given to prior work in human cytoarchitecture or macaque. Consideration of these details is important for the evaluation of the likelihood of the estimated sizes and positions of human auditory areas in a particular core/belt model.

Second, although many studies do present individual-subject data, the proposed organizations of cortical areas have been determined mostly from group-averaged data, which destroys key features of CFMs. Each CFM—in any sensory cortex—can vary dramatically in size and anatomical location across individuals, leading to shifts in cytoarchitectural and topographic boundaries (Clarke & Morosan 2012; Dougherty et al. 2003; Galaburda & Sanides 1980; Morosan et al. 2001; Rademacher et al. 1993, 2001; Schonwiesner et al. 2002). Consequently, relying on whole-brain anatomical coalignment for cortical averaging, as is typical in group-averaged data analysis, will cause different CFMs to be averaged together incorrectly into one measurement (for additional discussion of these problems, see Supplemental Materials Text and Supplemental Figure 4).

Finally, most studies have not been able to include alternate measures of functional differences between core and belt to estimate this set of boundaries, as these expected differences in human have not yet been established fully. Although there is good cytoarchitectural support of similarities between macaque STG (Fullerton & Pandya 2007, Galaburda & Sanides 1980, Hackett et al. 2001, Kaas & Hackett 2000) and human HG

(Clarke & Morosan 2012, Engel et al. 1994, Fullerton & Pandya 2007, Galaburda & Sanides 1980, Morosan et al. 2001), the functional homology between specific human and macaque auditory areas has not yet been determined adequately. Furthermore, only a few studies have correlated human tonotopy or other functional responses to human cytoarchitectural boundaries in the same subject, owing to the high difficulty of invasive measurements in human and the lack of noninvasive human neuroimaging alternatives until the very recent development of myelin-mapping magnetic resonance (MR) methods (Dick et al. 2012, Howard et al. 2000, Lutti et al. 2014, Moerel et al. 2014).

The majority of human tonotopic fMRI data show a similar pattern of organization with a low-frequency representation centered on HG. This central low representation is typically marked as the boundary for hA1 and hR (Figure 4). In some tonotopic studies (and in those with combined tonotopic and periodotopic measurements, as described below), this low-frequency region is surrounded by increasingly higher frequencies represented in bands forming a roughly circular shape (Figure 4a,d; Barton et al. 2012, Striem-Amit et al. 2011, Talavage et al. 2004). In others, portions of the circular high representation appear to be measured only weakly, such that the higher-frequency bands approximately resemble a horseshoe shape off the tip of HG that bends around the low-frequency region along HG's length (Figure 4b,c,e,f; Da Costa et al. 2011; Dick et al. 2012; Formisano et al. 2003; Humphries et al. 2010; Moerel et al. 2012, 2014; Santoro et al. 2014; Thomas et al. 2015; Upadhyay et al. 2007; Woods et al. 2010).

Studies also have varied widely in how many and which cortical areas from core and belt are named specifically within their tonotopic gradients. Occasionally, naming schemes are adopted that do not follow the macaque terminology, but the majority of studies use the names of the 11 core and belt areas from the macaque model. These studies typically place hA1 either on the medial aspect (tip) of HG, as suggested by human cytoarchitecture, or on the posterior (toward PT) aspect of HG. Then, hR is placed variably on the lateral (toward STG) or anterior (toward planum polare) aspect of HG, depending on where the strongest (or most obvious) high-to-low-to-high tonotopic reversal pattern expected for core can be identified in the imaging data. Sometimes the high-to-low-to-high gradient reversal labeled as hA1-hR is a relatively straight path; in other cases, it is bent. Depending on the placement of these areas, researchers then often simply overlay the monkey model to name the remaining areas, resulting in either a medial (HG tip) to lateral (HG base at STG) axis of orientation, consistent with the human cytoarchitecture (Figure 4a–c; e.g., Dick et al. 2012; Moerel et al. 2012, 2014), or an anterior-posterior axis of orientation, mostly parallel to STG (Figure 4e,f; e.g., Humphries et al. 2010, Thomas et al. 2015, Upadhyay et al. 2007, Woods et al. 2010). In most of these studies, the group-averaged data upon which the expected macaque arrangement of areas were overlaid problematically lack the data for many voxels that would be needed to substantiate the organization. A few studies have been careful not to attribute specific area names to the measured gradients beyond estimates of hA1, as accurate AFM boundary definitions are impossible without the measurement of an orthogonal gradient (for additional discussion, see Supplemental Materials Text and Supplemental Figures 2–4; e.g., Talavage et al. 2004).

In a worthy attempt to combine tonotopic and structural measurements, Upadhyay et al. (2007) tied tonotopic responses to measures of white matter connectivity from diffusion tensor imaging (DTI). However, as DTI does not yet have the spatial resolution to differentiate white matter projections within or near the gray matter of the cortical sheet, these measurements defined gradients for hA1 and hR that appear to extend from quite posterior to HG (hA1) to anterior to HG (hR). This definition would apparently place the high-frequency representation of hA1, the boundary that is expected to border CM and CL normally near CiS, as starting in or near PT, which in turn puts the sizes of hA1 and hR on a scale much larger than and on an axis rotated from those expected from multiple other measures. The attempt to combine structural and functional MR measurements in auditory cortex has been more successful with newly emerging myelin-mapping MR methods, which can examine differences in myelination density within cortical lamina. These myelin-mapping methods have been used with tonotopic measurements in the same subjects to demonstrate a firmer location and axis for core running from the tip of HG (hA1) to the base at STG (hRT), with a core organization much closer to that expected from human cytoarchitecture (Figures 3f,g and 4b,c; Dick et al. 2012, Lutti et al. 2014, Moerel et al. 2014). In addition, Moerel et al. (2014) demonstrated some myelination differences along part of the core/lateral belt border. Although this is a promising start, myelin mapping has not yet been proved to be effective for differentiating all 11 individual areas in core and belt or for mapping myelin differences reliably in individual subjects without averaging; further developments in this noninvasive imaging technology are expected to greatly enhance its utility for CFM border confirmation.

PERIODOTOPY: THE SECOND DIMENSION OF AUDITORY FIELD MAPS

Owing to the frequency-based organization of the basilar membrane, the cochlea is typically considered to be a frequency analyzer, which has led to a primary focus on the spectral content of sound and the corresponding tonotopic organization of cortex. However, the temporal content of sound is also integral to auditory processing (for additional discussion, see Langner 1992, Shamma2001). Periodic modulations of the amplitude of sounds, also known as temporal envelope variations or beat frequencies, arise in sounds with two or more frequency components. If two such complex harmonic sounds are composed of different composite frequencies (i.e., have different spectral contents) but still have the same temporal envelope periodicity, then the two sounds will have the same perceptual pitch (Pantev et al. 1996, Schouten et al. 1962).

Such periodicity information is thought to be coded in the auditory nerve through neural activity time-locked to the periodicity of the amplitude modulation (e.g., the length of time from peak-to-peak of the temporal envelope; Langner et al. 2009). The temporally varying aspects of sound likely drive neurons that respond to the onset and offset of sounds with different refractory times as well as neurons selective for sounds of certain durations. Periodotopy thus refers to the topographic organization of periodicity-responsive neurons.

The First Evidence for Periodotopy as a Second, Orthogonal Dimension

Initial measures of orthogonal tonotopic and periodotopic representations in mammalian neural pathways were discovered in the inferior colliculus (IC) of the cat midbrain (Langner

& Schreiner 1988, Schreiner & Langner 1988). This pair of studies demonstrated that IC neurons were tuned not only to a specific pure-tone frequency but also to a specific amplitude-modulation (AM) period. These measurements were later duplicated in chinchilla IC (Langner et al. 2002). Soon thereafter, orthogonal representations of these two acoustic dimensions were measured in gerbil, with a nearly circular periodicity representation overlaid upon a nearly linear tonotopic representation (Schulze et al. 2002). In more recent studies, periodotopic gradients were discovered in cat PAC (Langner et al. 2009) and macaque IC (Baumann et al. 2011). These periodotopic gradients were determined in both cases to be in the same location as, but orthogonal to, the tonotopic gradients. Finally, human psychophysical studies indicate that there are separable filter banks (e.g., neurons with receptive fields of particular widths or specific basilar membrane tuning filters) not only for frequency spectra, as expected with the presence of tonotopy, but also for temporal information, as would be expected with the presence of periodotopy (Dau et al. 1997, Ewert & Dau 2000, Hsieh & Saberi 2010).

Periodotopic Organization and Auditory Field Maps in Human Auditory Cortex

Langner et al. (1997) first demonstrated the presence of orthogonal representations of frequency and periodicity in human auditory cortex using magnetoencephalography (MEG). These MEG data of responses of pure-tone and harmonic stimuli were able to determine the orthogonality of the representations of these two dimensions, but the spatial resolution of the MEG measurements was not high enough to delineate individual AFMs or divisions among core, belt, and parabelt.

Inspired by these studies, Barton et al. (2012) recently used higher-resolution fMRI measurements in individual subjects to measure both tonotopic and periodotopic gradients around human PAC. These measurements showed that tonotopic representations are organized with a primary circular gradient positioned on HG, running from low-tone representations at the center to high-tone representations at the outer edge (Figure 5a,c). Two other mostly circular tonotopic representations abut this primary tonotopic gradient at the tip and base of HG, with high-tone gradient reversals present at each circular border. Thus far, only partial sections of these two tonotopic gradients have been analyzed in terms of core and belt, but it is expected from preliminary data that these measurements are only part of fully circular tonotopic representations. In contrast, the overlapping periodotopic representations are positioned as spokes on a wheel, with multiple gradients reversing back and forth around the circular and so-far-semicircular tonotopic representations (Figure 5b,d).

By identifying both tonotopic and periodotopic gradients in the same locations and measuring that these gradients were orthogonal to one another, Barton et al. (2012) were able to localize 11 independent AFMs that largely resemble the 11 AFMs of the monkey model (Figure 5a–d). Taking into account many characteristics of their data and the previously defined underlying cytoarchitecture, each of the AFMs was named based on those of the monkey model: hA1, hR, hRT, hCM, hMM, hRM, hRTM, hCL, hML, hAL, and hRTL. Because the monkey areas were named based on orientation and the human AFMs are oriented anatomically in a medial-lateral rather than caudal-rostraldirection, the human

AFMs are only the abbreviated letters, not the full title used by monkeys (e.g., hRM stands for human RM, not human rostral medial area).

hA1 lies at the tip of HG, is the largest of the 11 measured AFMs, and has the most detailed tonotopic and periodotopic gradients. The anterior/medial aspect of hA1 is tuned to high tones, and the posterior/lateral aspect is tuned to low tones (Figure 5a,c). The high-tone region of hA1 abuts the high-tone regions of hCM and hCL, forming a boundary reversal between these AFMs. Such tonotopic gradient reversals indicate the boundaries between hCM and hA1 (high tones), hCL and hA1 (high tones), hA1 and hR (low tones), and hR and hRT (high tones).

Periodotopic gradient reversals along HG divide the central circular tonotopic organization into two AFMs each of core, medial belt, and lateral belt: hA1, hR, hMM, hRM, hML, and hAL (Figure 5b,d). Just past the tip of HG and the high-tone reversal in CiS, a high-periodicity gradient reversal divides the second tonotopic representation into hCM and hCL. Similarly, at the base of HG and past another high-tone reversal, a set of periodotopic gradients divides the third tonotopic gradient into hRT, hRTM, and hRTL.

Running from the tip of HG to its base along STG, the set of three core AFMs is effectively identical to those measured in macaque electrophysiology and cytoarchitecture; all the tonotopic boundary reversals between hCM/hCL and hA1, hA1 and hR, and hR and hRT predicted by the monkey core model can be identified in human core (Figures 3 and 5a-d). Although periodotopic gradients had not yet been measured in macaque cortex, the measurements of Barton et al. (2012) of lateral and medial belt regions also generally followed the expected organization described by macaque cytoarchitecture, given the rotation of PAC from STG in macaque to HG in human. Similarly, the measurements of these 11 human AFMs are also consistent in terms of size, orientation, and boundaries with the previous human cytoarchitectural measurements. Thus, these human AFMs closely follow the correspondences among human cytoarchitecture, macaque cytoarchitecture, and macaque cortical auditory areas described above under the section entitled Cytoarchitecture in Auditory Cortex (for discussion of the differences between CFMs and cortical areas, see Supplemental Materials Text).

To date, one subsequent fMRI study in human cortex has also confirmed the orthogonal relationship between tonotopy and periodotopy (Figure 5e,f; Herdener et al. 2013). Unlike the individual-subject measurements of Barton et al. (2012), however, the group-averaged analysis used by Herdener et al. (2013) did not provide sufficient spatial resolution to measure specific AFMs accurately. The data they presented suggest that the hA1 and R AFMs are both much larger than expected from human cytoarchitectural measures and oriented perpendicular to what would be expected by a rotation of PAC from STG in macaque to HG in human. As described above and in the Supplemental Materials Text, the high variability of CFM sizes and positions with respect to the cortical gyri and sulci preclude analysis using whole-brain alignment and group averaging (Clarke & Morosan 2012; Dougherty et al. 2003; Galaburda & Sanides 1980; Morosan et al. 2001; Rademacher et al. 1993, 2001; Schonwiesner et al. 2002). The enlarged and incorrectly positioned AFMs from Herdener et al. (2013) actually demonstrate the expected outcome of averaging

together measurements of CFMs of various sizes and locations, as established for measurements of VFMs (Brewer et al. 2002, 2005; Dougherty et al. 2003; Wade et al. 2002; Wandell et al. 2005, 2007; Wandell & Winawer 2010).

A second and very recent human fMRI study similarly attempted to measure AFMs but failed to measure orthogonal periodotopic representations overlapping HG (Leaver & Rauschecker 2016). The issues encountered with this study exemplify the need for very careful and accurate cortical field mapping methods. The spatial resolution of these data was reduced greatly not only through group averaging across subjects but also by additional smoothing of the data for what appears to be at least three times per data set—once in image processing, once when determining voxel significance, and once when stimulus preference maps were generated. Furthermore, this study used a low-power experimental design by presenting stimuli in pseudorandom order rather than using a phase-encoded paradigm during data acquisition and also failed to use an appropriate statistical threshold for data analysis (Wandell et al. 2007). The resulting model is based only on tonotopy and does not correspond to either human cytoarchitectural measurements or to expected homology between human HG and macaque STG. Thus, it is important to remember that the failure to measure a CFM or a component gradient does not necessarily mean that a CFM does not exist in that location; as demonstrated here, there are many technical hurdles to overcome and perfect (for additional discussion of the importance of high-quality data acquisition and analysis, see Supplemental Materials Text; Brewer & Barton 2012; Brewer et al. 2005; Wandell et al. 2005, 2007).

Confirmation of Periodotopic Representations in Macaque Cortex

Following Barton et al.’s (2012) human AFM measurements, Baumann et al. (2015) measured orthogonal periodotopic gradients in macaque cortex (Figure 6). They were able to define hA1, R, and CL, positioned along STG consistent with expectations from macaque cytoarchitectural and electrophysiological measurements; their measurements were unable to resolve the other AFMs surrounding these, however. Figure 4a,b demonstrates the likely correspondence between the tonotopic and periodotopic representations underlying these three AFMs in macaque and human.

The exact homology between human and macaque is not yet clear and will require comparison of functional selectivity between specific AFMs. Such commonalities between tonotopic and periodotopic boundaries and cytoarchitectural measurements in each species strongly support the rotation of PAC from STG in macaque to HG in human. As in visual measurements, macaque measurements of AFMs can be very useful in the exploration of human auditory cortex, but we should not assume that the monkey model is a correct representation of the human organization. Rather, the monkey model should be viewed as an especially useful rough model of human cortex, where differences are also expected (for additional discussion of cross-species comparisons, see Supplemental Materials Text and Supplemental Figure 6).

MACROSTRUCTURAL ORGANIZATION OF AUDITORY FIELD MAPS

Cloverleaf Clusters—With the emergence of evidence for extensive regions of CFMs across primate sensory cortices, attention has turned to whether these CFMs might be grouped on a larger (i.e., macrostructural) scale. Brewer and associates first described such a macrostructural organization in human visual cortex with VFMs grouped into clusters of CFMs, or cloverleaf clusters (Brewer & Barton 2012; Brewer et al. 2005; Wandell et al. 2005, 2007); subsequent measurements demonstrated the presence of these clusters in other parts of human visual cortex (Kolster et al. 2010), in macaque visual cortex (Kolster et al. 2009), and now in human auditory cortex (Barton et al. 2012). Cloverleaf clusters are composed of groups of CFMs; one dimension of sensory topography (e.g., tonotopy) is represented in concentric, circular bands from center to periphery of the cluster, and the second orthogonal dimension (e.g., periodotopy) divides this confluent representation up into multiple maps with radial bands spanning the cluster center to periphery (Figure 5). The spatial organization of the CFMs may not only be important for the definition of CFMs but may also play a role in coordinating neural computations (for additional discussion of cloverleaf clusters, see Supplemental Materials Texts and Supplemental Figure 5).

The first auditory cloverleaf cluster—the HG cluster—is centered on the primary, circular tonotopic gradient on HG and consists of six AFMs (hA1, hAL, hML, hR, hRM, and hMM; Barton et al. 2012). Isotone bands are organized in concentric circles with central low-tone representations surrounded by increasingly higher tone bands, whereas isoperiod bands extend from the center to the periphery of the cluster like spokes on a wheel. Abutting the cluster where HG meets STG, there exists a tonotopic reversal into three additional AFMs (hRT, hRTL, and hRTM). Similarly, two more AFMs abut the HG cluster medially (hCM and hCL). We suspect that these two sets of AFMs each also form one part of a complete cloverleaf cluster; more research is required to determine whether this is the case.

CONCLUSIONS

Armed with this foundational knowledge of the number, location, and organization of AFMs in human auditory core and belt, future research can be directed to localizing higher-order AFMs and determining which computations are performed in each AFM. The understanding of this underlying organization will give us insights into the computational inputs to higher auditory and language processing. Interestingly, both auditory and visual regions of human cortex share a common organizational scheme, with each sensory system compartmentalized into CFMs that are themselves arranged on a larger scale into cloverleaf clusters. Such similarity may be a common organizational structure across many sensory systems, which may aid in the future identification of CFMs in the representations of other senses.

Supplementary Material

Refer to Web version on PubMed Central for supplementary material.

ACKNOWLEDGMENTS

We thank Professor Greg Hickok, Professor Kourosh Saberi, and Dr. Jon Venezia for their collaborative work with us in our investigations into the organization of auditory cortex. Work in the A.A.B. Laboratory for Visual

Neuroscience is supported in part by research grant #1329255 from the National Science Foundation Cognitive Sciences Program; by research grant #1413417 from the National Science Foundation Mathematical Biology Program; by research grant #L30 EY019249 from the National Institutes of Health (NIH); by a pilot grant from the Center for Hearing Research at the University of California, Irvine (UCI); and by startup funds from the UCI Department of Cognitive Sciences. The A.A.B. laboratory also relies on resources from the UCI Institute for Clinical and Translational Sciences, which is supported by the National Center for Research Resources and the National Center for Advancing Translational Sciences at the NIH through grant UL1 TR001414. The content is solely the responsibility of the authors and does not necessarily represent the official views of the NIH. B.B. is supported by a postdoctoral fellowship through research grant #1329255 from the National Science Foundation Cognitive Sciences Program.

Glossary

MGN
medial geniculate nucleus (of the thalamus)

PAC
primary auditory cortex, also known as auditory core

STG
superior temporal gyrus

HG
Heschl's gyrus

Orthogonal dimensions
independent sensory space measurements with gradient vectors for each dimension at right angles to each other

CFM
cortical field map

VFM
visual field map

AFM
auditory field Map

V1
primary visual cortex; visual area 1

fMRI
functional magnetic resonance imaging

macaque medial belt
cortical region comprising CM (caudal medial area), RM (rostral medial area), and RTM (medial rostral temporal area)

macaque lateral belt
cortical region comprising CL (caudal lateral area), ML(middle lateral area), AL (anterior lateral area), and RTL (lateral rostral temporal area)

macaque parabelt
cortical region comprising RPB (rostral parabelt) and CPB (caudal parabelt)

macaque PAC
cortical region comprising A1 (auditory area 1), R (rostral area), and RT (rostral temporal area)

hA1
first human auditory area, likely corresponding to macaque auditory area 1 (A1)

hA1, hR, and hRT
three cortical areas composing human auditory core or PAC, named for anatomical directions in macaque

hCM, hMM, hRM, and hRTM
four cortical areas that compose human auditory medial belt, named for anatomical directions in macaque

hCL, hML, hAL, and hRTL
four cortical areas that compose human auditory lateral belt, named for anatomical directions in macaque

LITERATURE CITED

Amunts K, Malikovic A, Mohlberg H, Schormann T, Zilles K. 2000 Brodmann's areas 17 and 18 brought into stereotaxic space—where and how variable? Neuroimage 11:66–84 [PubMed: 10686118]

Amunts K, Schleicher A, Burgel U, Mohlberg H, Uylings HB, Zilles K. 1999 Broca's region revisited: cytoarchitecture and intersubject variability. J. Comp. Neurol. 412:319–41 [PubMed: 10441759]

Barton B, Venezia JH, Saberi K, Hickok G, Brewer AA. 2012 Orthogonal acoustic dimensions define auditory field maps in human cortex. PNAS 109:20738–43 [PubMed: 23188798]

Baumann S, Griffiths TD, Sun L, Petkov CI, Thiele A, Rees A. 2011 Orthogonal representation of sound dimensions in the primate midbrain. Nat. Neurosci. 14:423–25 [PubMed: 21378972]

Baumann S, Joly O, Rees A, Petkov CI, Sun L, et al. 2015 The topography of frequency and time representation in primate auditory cortices. eLife 4:e03256

Brewer AA, Barton B. 2012 Visual field map organization in human visual cortex In *Visual Cortex: Current Status and Perspectives*, ed. Molotchnikoff S, Rouat J, pp. 29–60. Rijeka, Croat.: InTech

Brewer AA, Liu J, Wade AR, Wandell BA. 2005 Visual field maps and stimulus selectivity in human ventral occipital cortex. Nat. Neurosci. 8:1102–9 [PubMed: 16025108]

Brewer AA, Press WA, Logothetis NK, Wandell BA. 2002 Visual areas in macaque cortex measured using functional magnetic resonance imaging. J. Neurosci. 22:10416–26 [PubMed: 12451141]

Chklovskii DB, Koulakov AA. 2004 Maps in the brain: What can we learn from them? Annu. Rev. Neurosci. 27:369–92 [PubMed: 15217337]

Clarke S, Morosan P. 2012 Architecture, connectivity, and transmitter receptors of human auditory cortex In The Human Auditory Cortex, ed. Poeppel D, Overath T, Popper AN, Richard RR, pp. 11–38. New York: Springer

Da Costa S, van der Zwaag W, Marques JP, Frackowiak RSJ, Clarke S, Saenz M. 2011 Human primary auditory cortex follows the shape of Heschl's gyrus. J. Neurosci. 31:14067–75 [PubMed: 21976491]

Dau T, Kollmeier B, Kohlrausch A. 1997 Modeling auditory processing of amplitude modulation. II. Spectral and temporal integration. J. Acoust. Soc. Am. 102:2906–19 [PubMed: 9373977]

de la Mothe LA, Blumell S, Kajikawa Y, Hackett TA. 2006 Cortical connections of the auditory cortex in marmoset monkeys: core and medial belt regions. J. Comp. Neurol. 496:27–71 [PubMed: 16528722]

DeYoe EA, Carman GJ, Bandettini P, Glickman S, Wieser J, et al. 1996 Mapping striate and extrastriate visual areas in human cerebral cortex. PNAS 93:2382–86 [PubMed: 8637882]

Dick F, Tierney AT, Lutti A, Josephs O, Sereno MI, Weiskopf N. 2012 In vivo functional and myeloarchitectonic mapping of human primary auditory areas. J. Neurosci. 32:16095–105 [PubMed: 23152594]

Dougherty RF, Koch VM, Brewer AA, Fischer B, Modersitzki J, Wandell BA. 2003 Visual field representations and locations of visual areas V1/2/3 in human visual cortex. J. Vis. 3:586–98 [PubMed: 14640882]

Engel SA, Glover GH, Wandell BA. 1997 Retinotopic organization in human visual cortex and the spatial precision of functional MRI. Cereb. Cortex 7:181–92 [PubMed: 9087826]

Engel SA, Rumelhart DE, Wandell BA, Lee AT, Glover GH, et al. 1994 fMRI of human visual cortex. Nature 369:525 [PubMed: 8031403]

Ewert SD, Dau T. 2000 Characterizing frequency selectivity for envelope fluctuations. J. Acoust. Soc. Am. 108:1181–96 [PubMed: 11008819]

Formisano E, Kim DS, Di Salle F, van de Moortele PF, Ugurbil K, Goebel R. 2003 Mirror-symmetric tonotopic maps in human primary auditory cortex. Neuron 40:859–69 [PubMed: 14622588]

Fullerton BC, Pandya DN. 2007 Architectonic analysis of the auditory-related areas of the superior temporal region in human brain. J. Comp. Neurol. 504:470–98 [PubMed: 17701981]

Galaburda AM, Pandya DN. 1983 The intrinsic architectonic and connectional organization of the superior temporal region of the rhesus monkey. J. Comp. Neurol. 221:169–84 [PubMed: 6655080]

Galaburda AM, Sanides F. 1980 Cytoarchitectonic organization of the human auditory cortex. J. Comp. Neurol. 190:597–610 [PubMed: 6771305]

Hackett TA. 2011 Information flow in the auditory cortical network. Hear. Res. 271:133–46 [PubMed: 20116421]

Hackett TA, Preuss TM, Kaas JH. 2001 Architectonic identification of the core region in auditory cortex of macaques, chimpanzees, and humans. J. Comp. Neurol. 441:197–222 [PubMed: 11745645]

Hackett TA, Stepniewska I, Kaas JH. 1998a Subdivisions of auditory cortex and ipsilateral cortical connections of the parabelt auditory cortex in macaque monkeys. J. Comp. Neurol. 394:475–95 [PubMed: 9590556]

Hackett TA, Stepniewska I, Kaas JH. 1998b Thalamocortical connections of the parabelt auditory cortex in macaque monkeys. J. Comp. Neurol. 400:271–86 [PubMed: 9766404]

Hedges S, Kumar S. 2003 Genomic clocks and evolutionary timescales. Trends Genet. 19:200–6 [PubMed: 12683973]

Herdener M, Esposito F, Scheffler K, Schneider P, Logothetis NK, et al. 2013 Spatial representations of temporal and spectral sound cues in human auditory cortex. Cortex 49:2822–33 [PubMed: 23706955]

Howard MA, Volkov IO, Mirsky R, Garell PC, Noh MD, et al. 2000 Auditory cortex on the human posterior superior temporal gyrus. J. Comp. Neurol. 416:79–92 [PubMed: 10578103]

Hsieh IH, Saberi K. 2010 Detection of sinusoidal amplitude modulation in logarithmic frequency sweeps across wide regions of the spectrum. Hear. Res. 262:9–18 [PubMed: 20144700]

Humphries C, Liebenthal E, Binder JR. 2010 Tonotopic organization of human auditory cortex. Neuroimage 50:1202–11 [PubMed: 20096790]

Joly O, Baumann S, Balezeau F, Thiele A, Griffiths TD. 2014 Merging functional and structural properties of the monkey auditory cortex. Front. Neurosci. 8:198 [PubMed: 25100930]

Jones EG, Dell'Anna ME, Molinari M, Rausell E, Hashikawa T. 1995 Subdivisions of macaque monkey auditory cortex revealed by calcium-binding protein immunoreactivity. J. Comp. Neurol. 362:153–70 [PubMed: 8576431]

Kaas JH. 1997 Topographic maps are fundamental to sensory processing. Brain Res. Bull. 44:107–12 [PubMed: 9292198]

Kaas JH, Hackett TA. 2000 Subdivisions of auditory cortex and processing streams in primates. PNAS 97:11793–99 [PubMed: 11050211]

Kajikawa Y, Frey S, Ross D, Falchier A, Hackett TA, Schroeder CE. 2015 Auditory properties in the parabelt regions of the superior temporal gyrus in the awake macaque monkey: an initial survey. J. Neurosci. 35:4140–50 [PubMed: 25762661]

Kolster H, Mandeville JB, Arsenault JT, Ekstrom LB, Wald LL, Vanduffel W. 2009 Visual field map clusters in macaque extrastriate visual cortex. J. Neurosci. 29:7031–39 [PubMed: 19474330]

Kolster H, Peeters R, Orban GA. 2010 The retinotopic organization of the human middle temporal area MT/V5 and its cortical neighbors. J. Neurosci. 30:9801–20 [PubMed: 20660263]

Kosaki H, Hashikawa T, He J, Jones EG. 1997 Tonotopic organization of auditory cortical fields delineated by parvalbumin immunoreactivity in macaque monkeys. J. Comp. Neurol. 386:304–16 [PubMed: 9295154]

Krubitzer LA, Seelke AM. 2012 Cortical evolution in mammals: the bane and beauty of phenotypic variability. PNAS 109:10647–54 [PubMed: 22723368]

Kusmierek P, Rauschecker JP. 2009 Functional specialization of medial auditory belt cortex in the alert rhesus monkey. J. Neurophysiol. 102:1606–22 [PubMed: 19571201]

Langner G 1992 Periodicity coding in the auditory system. Hear. Res. 60:115–42 [PubMed: 1639723]

Langner G, Albert M, Briede T. 2002 Temporal and spatial coding of periodicity information in the inferior colliculus of awake chinchilla *(Chinchilla laniger)*. Hear. Res. 168:110–30 [PubMed: 12117514]

Langner G, Dinse HR, Godde B. 2009 A map of periodicity orthogonal to frequency representation in the cat auditory cortex. Front. integr. Neurosci. 3:27 [PubMed: 19949464]

Langner G, Sams M, Heil P, Schulze H. 1997 Frequency and periodicity are represented in orthogonal maps in the human auditory cortex: evidence from magnetoencephalography. J. Comp. Physiol. A 181:665–76 [PubMed: 9449825]

Langner G, Schreiner CE. 1988 Periodicity coding in the inferior colliculus of the cat. I. Neuronal mechanisms. J. Neurophysiol. 60:1799–822 [PubMed: 3236052]

Leaver AM, Rauschecker JP. 2016 Functional topography of human auditory cortex. J. Neurosci. 36:1416–28 [PubMed: 26818527]

Leonard CM, Puranik C, Kuldau JM, Lombardino LJ. 1998 Normal variation in the frequency and location of human auditory cortex landmarks. Heschl's gyrus: Where is it? Cereb. Cortex 8:397–406 [PubMed: 9722083]

Lutti A, Dick F, Sereno MI, Weiskopf N. 2014 Using high-resolution quantitative mapping of R1 as an index of cortical myelination. Neuroimage 93(Pt. 2):176–88 [PubMed: 23756203]

Merzenich MM, Brugge JF. 1973 Representation of the cochlear partition of the superior temporal plane of the macaque monkey. Brain Res. 50:275–96 [PubMed: 4196192]

Mitchison G 1991 Neuronal branching patterns and the economy of cortical wiring. Proc. Biol. Sci. 245:151–8 [PubMed: 1682939]

Moerel M, De Martino F, Formisano E. 2012 Processing of natural sounds in human auditory cortex: tonotopy, spectral tuning, and relation to voice sensitivity. J. Neurosci. 32:14205–16 [PubMed: 23055490]

Moerel M, De Martino F, Formisano E. 2014 An anatomical and functional topography of human auditory cortical areas. Front. Neurosci. 8:225 [PubMed: 25120426]

Molinari M, Dell'Anna ME, Rausell E, Leggio MG, Hashikawa T, Jones EG. 1995 Auditory thalamocortical pathways defined in monkeys by calcium-binding protein immunoreactivity. J. Comp. Neurol. 362:171–94 [PubMed: 8576432]

Moradi F, Heeger DJ. 2009 Inter-ocular contrast normalization in human visual cortex. J. Vis. 9:13

Morel A, Garraghty PE, Kaas JH. 1993 Tonotopic organization, architectonic fields, and connections of auditory cortex in macaque monkeys. J. Comp. Neurol. 335:437–59 [PubMed: 7693772]

Morosan P, Rademacher J, Schleicher A, Amunts K, Schormann T, Zilles K. 2001 Human primary auditory cortex: cytoarchitectonic subdivisions and mapping into a spatial reference system. Neuroimage 13:684–701 [PubMed: 11305897]

Pandya DN, Sanides F. 1973 Architectonic parcellation of the temporal operculum in rhesus monkey and its projection pattern. Z. Anatom. Entwickl. 139:127–61

Pantev C, Elbert T, Ross B, Eulitz C, Terhardt E. 1996 Binaural fusion and the representation of virtual pitch in the human auditory cortex. Hear. Res. 100:164–70 [PubMed: 8922991]

Petkov CI, Kayser C, Augath M, Logothetis NK. 2006 Functional imaging reveals numerous fields in the monkey auditory cortex. PLOS Biol. 4:e215 [PubMed: 16774452]

Petkov CI, Kayser C, Augath M, Logothetis NK. 2009 Optimizing the imaging of the monkey auditory cortex: sparse versus continuous fMRI. Magn. Reson. Imaging 27:1065–73 [PubMed: 19269764]

Press WA, Brewer AA, Dougherty RF, Wade AR, Wandell BA. 2001 Visual areas and spatial summation in human visual cortex. Vision Res. 41:1321–32 [PubMed: 11322977]

Rademacher J, Caviness VS, Jr., Steinmetz H, Galaburda AM. 1993 Topographical variation of the human primary cortices: implications for neuroimaging, brain mapping, and neurobiology. Cereb. Cortex 3:313–29 [PubMed: 8400809]

Rademacher J, Morosan P, Schormann T, Schleicher A, Werner C, et al. 2001 Probabilistic mapping and volume measurement of human primary auditory cortex. NeuroImage 13:669–83 [PubMed: 11305896]

Rauschecker JP, Tian B. 2004 Processing of band-passed noise in the lateral auditory belt cortex of the rhesus monkey. J. Neurophysiol. 91:2578–89 [PubMed: 15136602]

Rauschecker JP, Tian B, Hauser M. 1995 Processing of complex sounds in the macaque nonprimary auditory cortex. Science 268:111–4 [PubMed: 7701330]

Recanzone GH, Guard DC, Phan ML. 2000 Frequency and intensity response properties of single neurons in the auditory cortex of the behaving macaque monkey. J. Neurophysiol. 83:2315–31 [PubMed: 10758136]

Rivier F, Clarke S. 1997 Cytochrome oxidase, acetylcholinesterase, and NADPH-diaphorase staining in human supratemporal and insular cortex: evidence for multiple auditory areas. NeuroImage 6:288–304 [PubMed: 9417972]

Romanski LM, Bates JF, Goldman-Rakic PS. 1999 Auditory belt and parabelt projections to the prefrontal cortex in the rhesus monkey. J. Comp. Neurol. 403:141–57 [PubMed: 9886040]

Saenz M, Langers DR. 2014 Tonotopic mapping of human auditory cortex. Hear. Res. 307:42–52 [PubMed: 23916753]

Sanchez-Panchuelo RM, Francis S, Bowtell R, Schluppeck D. 2010 Mapping human somatosensory cortex in individual subjects with 7T functional MRI. J. Neurophysiol. 103:2544–56 [PubMed: 20164393]

Santoro R, Moerel M, De Martino F, Goebel R, Ugurbil K, et al. 2014 Encoding of natural sounds at multiple spectral and temporal resolutions in the human auditory cortex. PLOS Comp. Biol. 10:e1003412

Schonwiesner M, von Cramon DY, Rubsamen R. 2002 Is it tonotopy after all? NeuroImage 17:1144–61 [PubMed: 12414256]

Schouten J, Ritsma R, Cardozo B. 1962 Pitch of the residue. J. Acornt. Soc. Am. 34:1418–24

Schreiner CE, Langner G. 1988 Periodicity coding in the inferior colliculus of the cat. II. Topographical organization. J. Neurophysiol. 60:1823–40 [PubMed: 3236053]

Schulze H, Hess A, Ohl FW, Scheich H. 2002 Superposition of horseshoe-like periodicity and linear tonotopic maps in auditory cortex of the Mongolian gerbil. Eur. J. Neurosci. 15:1077–84 [PubMed: 11918666]

Sereno MI, Dale AM, Reppas JB, Kwong KK, Belliveau JW, et al. 1995 Borders of multiple visual areas in humans revealed by functional magnetic resonance imaging. Science 268:889–93 [PubMed: 7754376]

Shamma S 2001 On the role of space and time in auditory processing. Trends Cogn. Sci. 5:340–48 [PubMed: 11477003]

Shapley R, Hawken M, Xing D. 2007 The dynamics of visual responses in the primary visual cortex. Prog. Brain Res. 165:21–32 [PubMed: 17925238]

Striem-Amit E, Hertz U, Amedi A. 2011 Extensive cochleotopic mapping of human auditory cortical fields obtained with phase-encoding fMRI. PLOS ONE 6:e17832 [PubMed: 21448274]

Sweet RA, Dorph-Petersen KA, Lewis DA. 2005 Mapping auditory core, lateral belt, and parabelt cortices in the human superior temporal gyrus. J. Comp. Neurol. 491:270–89 [PubMed: 16134138]

Talavage TM, Sereno MI, Melcher JR, Ledden PJ, Rosen BR, Dale AM. 2004 Tonotopic organization in human auditory cortex revealed by progressions of frequency sensitivity. J. Neurophysiol. 91:1282–96 [PubMed: 14614108]

Tanji K, Leopold DA, Ye FQ, Zhu C, Malloy M, et al. 2010 Effect of sound intensity on tonotopic fMRI maps in the unanesthetized monkey. NeuroImage 49:150–57 [PubMed: 19631273]

Thomas JM, Huber E, Stecker GC, Boynton GM, Saenz M, Fine I. 2015 Population receptive field estimates of human auditory cortex. NeuroImage 105:428–39 [PubMed: 25449742]

Tian B, Rauschecker JP. 2004 Processing of frequency-modulated sounds in the lateral auditory belt cortex of the rhesus monkey. J. Neurophysiol. 92:2993–3013 [PubMed: 15486426]

Upadhyay J, Ducros M, Knaus TA, Lindgren KA, Silver A, et al. 2007 Function and connectivity in human primary auditory cortex: a combined fMRI and DTI study at 3 Tesla. Cereb. Cortex 17:2420–32 [PubMed: 17190967]

Van Essen DC. 2003 Organization of visual areas in macaque and human cerebral cortex In The Visual Neurosciences, ed. Chalupa LM Werner JS, pp. 507–21. Boston: Bradford Books

von Economo C, Koskinas GN. 1925 Die Cytoarchitectonik der Hirnrinde des erwachsenen Menschen. Berlin: Julius-Springer

Wade AR, Brewer AA, Rieger JW, Wandell BA. 2002 Functional measurements of human ventral occipital cortex: retinotopy and colour. Philos. Trans. R. Soc. B 57:963–73

Wandell BA, Brewer AA, Dougherty RF. 2005 Visual field map clusters in human cortex. Philos. Trans. R. Soc. B 360:693–707

Wandell BA, Dumoulin SO, Brewer AA. 2007 Visual field maps in human cortex. Neuron 56:366–83 [PubMed: 17964252]

Wandell BA, Winawer J. 2010 Imaging retinotopic maps in the human brain. Vision Res. 51:718–37 [PubMed: 20692278]

Wessinger CM, VanMeter J, Tian B, Van LareJ, Pekar J, Rauschecker JP. 2001 Hierarchical organization of the human auditory cortex revealed by functional magnetic resonance imaging. J. Cog. Neurosci. 13:1–7

Woods DL, Herron TJ, Cate AD, Yund EW, Stecker GC, et al.2010 Functional properties of human auditory cortical fields. Front. Syst. Neurosci. 4:155 [PubMed: 21160558]

Zeki S 2003 Improbable areas in the visual brain. Trends Neurosci. 26:23–26 [PubMed: 12495859]

Zeki S, Bartels A. 1999 Toward a theory of visual consciousness. Conscious. Cogn. 8:225–59 [PubMed: 10448004]

SUMMARY POINTS

1. Cortical field maps (CFMs) require the measurement of two orthogonal gradients representing two dimensions of sensory space.
2. The two dimensions used to measure auditory field maps (AFMs) are tonotopy and periodotopy, representing spectral and temporal aspects of audition, respectively.
3. Eleven AFMs have been measured in human auditory cortex, composing core and belt regions with likely homology to the similarly named cortical areas in macaque.
4. On a macrostructural scale, AFMs are organized into groups called cloverleaf clusters, which have also been measured in human and macaque visual cortex.

FUTURE ISSUES

1. What are the extent and organization of AFMs outside of human core and belt regions?
2. At what point, if any, does a difference in AFM organization develop between the hemispheres?
3. What functional computations are performed throughout the cortical hierarchy of AFMs?
4. Is the subcortical organization of auditory pathways in human similar to that of macaque?
5. How do AFM organization and functionality compare between macaque and human?
6. To what extent do changes in auditory attention affect the tuning of tonotopy and peri-odotopy in core and belt AFMs?
7. Are other acoustic features represented as gradients across auditory cortex?
8. How are tonotopic (spectral) and periodotopic (temporal) features used as inputs into higher order regions subserving speech production and language comprehension?

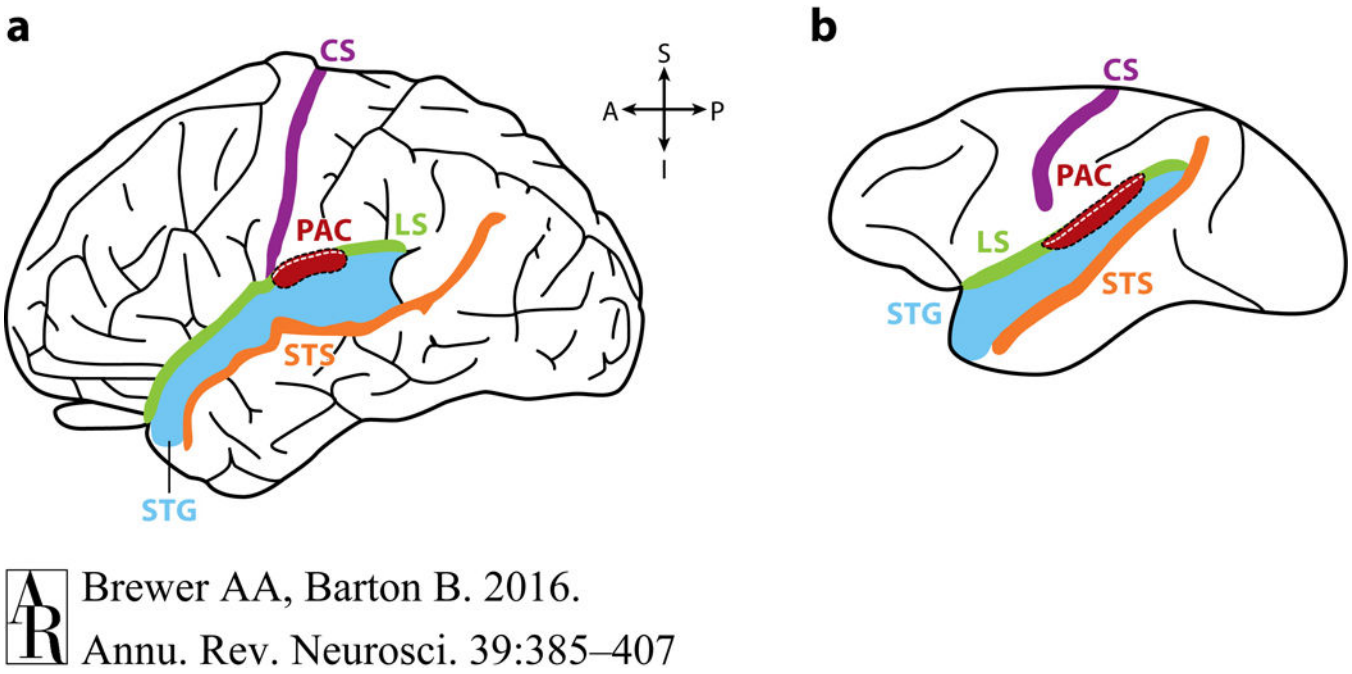

Brewer AA, Barton B. 2016.
Annu. Rev. Neurosci. 39:385–407

Figure 1.

Primary auditory cortex. (*a*) Diagram of the lateral view of the human left cerebral hemisphere. Black lines denote major sulci. The general location of PAC is marked in red within the black dotted line. The white dotted line within this region denotes the extension of PAC into LS along Heschl's gyrus that is not visible in this view. (*b*) Diagram of the lateral view of the macaque monkey left cerebral hemisphere. The general location of PAC is again marked in red within the black dotted line. The white dotted line within this region denotes the extension of PAC along the posterior bank of LS. Inset shows anatomical directions (S, superior; I, inferior; A, anterior; P, posterior). Abbreviations: CS, central sulcus (*purple*); LS, lateral sulcus, also known as the lateral or Sylvian fissure (*green*); PAC, primary auditory cortex (*red*); STG, superior temporal gyrus (*blue*); STS, superior temporal sulcus (*orange*).

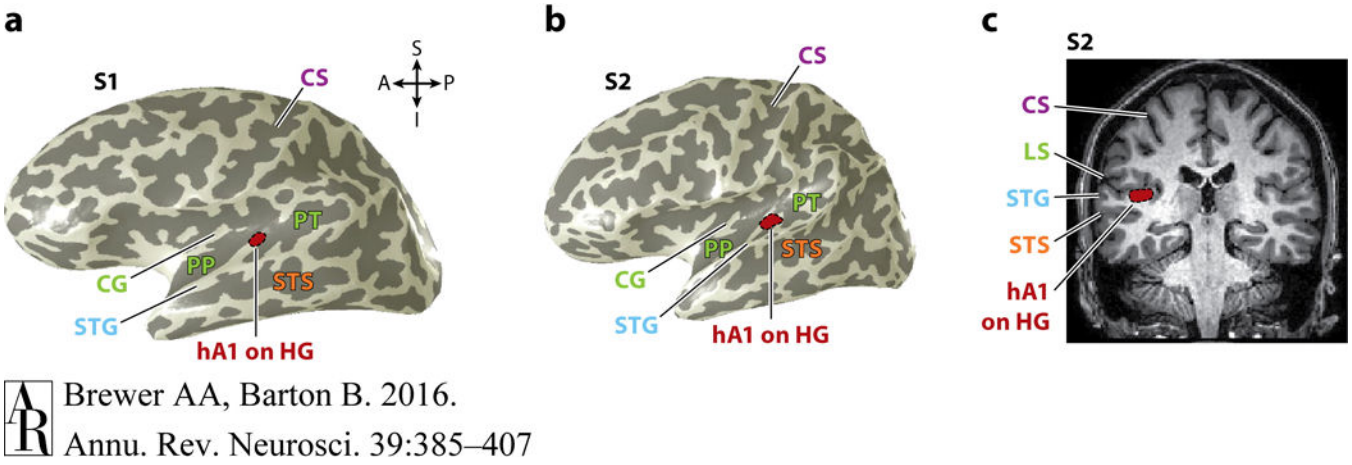

Brewer AA, Barton B. 2016.
Annu. Rev. Neurosci. 39:385–407

Figure 2.

hA1 and Heschl's gyrus. (*a,b*) Three-dimensional renderings of individual cortical surfaces. Light gray indicates gyrus; dark gray indicates sulcus. The specific location of the hA1 cortical field map for each subject is marked in red within the black dotted lines. In both typical subjects, hA1 lies at the tip of HG. Note that HG in S1 (*a*) is a single gyrus, whereas HGin S2 (*b*) has a double peak, seen here as two light gray stripes. (*c*) A coronal view of hA1 on HG (*red* within *dotted black line*) is shown for S2. Inset shows anatomical directions (S, superior; I, inferior; A, anterior; P, posterior). Abbreviations: CG, circular gyrus (green); CS, central sulcus (*purple*); hA1, first human auditory area (*red*); HG, Heschl's gyrus (*red*); PP, planum polare (*green*); PT, planum temporale (*green*); STG, superior temporal gyrus (*blue*); STS, superior temporal sulcus (*orange*). Green labels are sections within the lateral sulcus (LS) (shown in Figure 1).

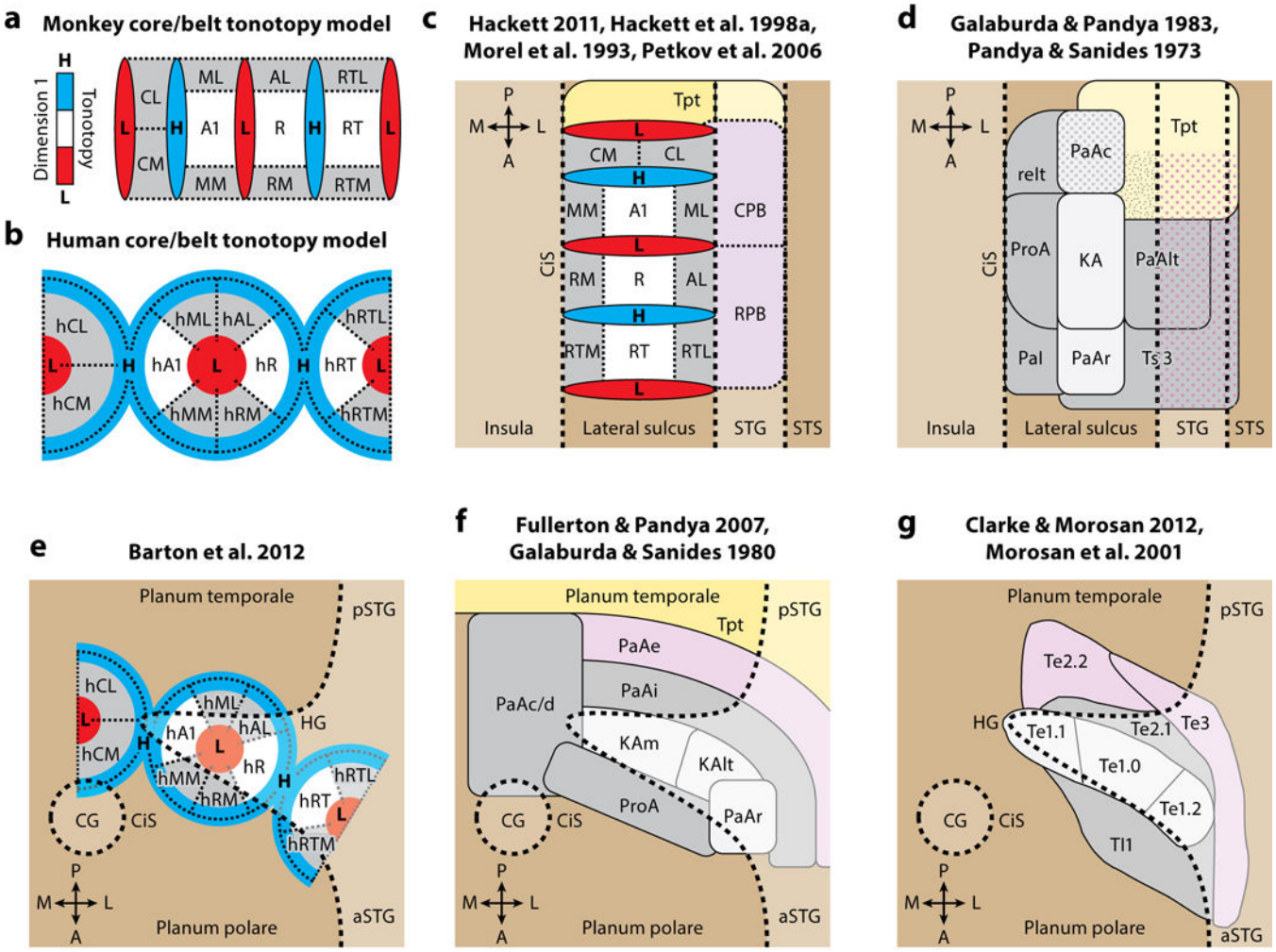

Brewer AA, Barton B. 2016.
Annu. Rev. Neurosci. 39:385–407

Figure 3.

Model comparisons: macaque and human tonotopy and cytoarchitecture. (*a*) Schematic diagram shows tonotopic representations overlaid along the core and belt regions of macaque auditory cortex. L and H refer to low (*red*) or high (*blue*) tonotopic responses, respectively. Core areas (A1, R, RT) are shown in white, and belt areas (ML, AL, RTL, RTM, RM, MM, CM, CL) are shown in gray. (*b*) Schematic diagram shows tonotopic representations overlaid along the core (*white*) and belt (*gray*) cortical field maps of human auditory cortex, as defined by Barton et al. (2012). (*c-g*) Models of macaque and human auditory area organization overlaid on flattened sections of cortex. Darker beige background indicates sulci or the plane of the lateral sulcus, whereas lighter beige overlay indicates gyri. Purple regions indicate parabelt areas. Yellow regions indicate cytoarchitectonic area Tpt within PT. Other colors as in panel *a*. All figures are oriented along the same global anatomical axes (see inset legends; M, medial; L, lateral; A, anterior; P, posterior). All models are representations of the original models cited above each figure panel, modified for comparative consistency here. (*c*) Model of macaque auditory core, belt, and parabelt

overlaid with high/low tonotopic gradient reversals. (*d*) Cytoarchitectonic model of monkey auditory cortex. The potential homology of the lateral portion of PaAlt and anterior/lateral Tpt to the parabelt in panel *c* is noted by the gray/purple dot pattern and yellow/purple dot pattern, respectively. Similarly, the potential homology of anterior/medial Tpt to lateral belt (e.g., ML) is noted by the yellow/gray pattern. Finally, the posterior region PaAc was grouped as a strip of core areas with KA and PaAr but is likely homologous to the belt regions in panel *c*, as noted by the gray/white dot pattern. (*e*) Model of human core and belt cortical field maps overlaid with high/low tonotopic representations. (*f,g*) Cytoarchitectonic models of human auditory cortex. Note the rotation of the likely homologous regions between species from STG to HG (homology noted by matching colors). Abbreviations: A1, first auditory area; AL, anterior lateral area; aSTG, anterior superior temporal gyrus; CG, circular gyrus; CiS, circular sulcus; CL, caudal lateral area; CM, caudal medial area; CPB, caudal parabelt; h, human; HG, Heschl's gyrus; KA, koniocortical area; KAlt, lateral koniocortical area; KAm, medial koniocortical area; ML, medial lateral area; MM, medial medial area; PaAc, caudal parakoniocortical area; PaAc/d, caudal-dorsal parakoniocortical area; PaAe, lateral parakoniocortical area, external; PaAi, lateral parakoniocortical area, internal; PaAlt, lateral parakoniocortical area; PaAr, rostral parakoniocortical area; PaI, parainsular area; ProA, prokoniocortical area; pSTG, posterior superior temporal gyrus; PT, planum temporale; R, rostral area; reIt, retroinsular area; RM, rostral medial area; RPB, rostral parabelt; RT, rostral temporal area; RTL, rostral temporal lateral area; RTM, rostral temporal medial area; STG, superior temporal gyrus; STS, superior temporal sulcus; Tpt, temporoparietal area; Ts3, temporalis superior 3.

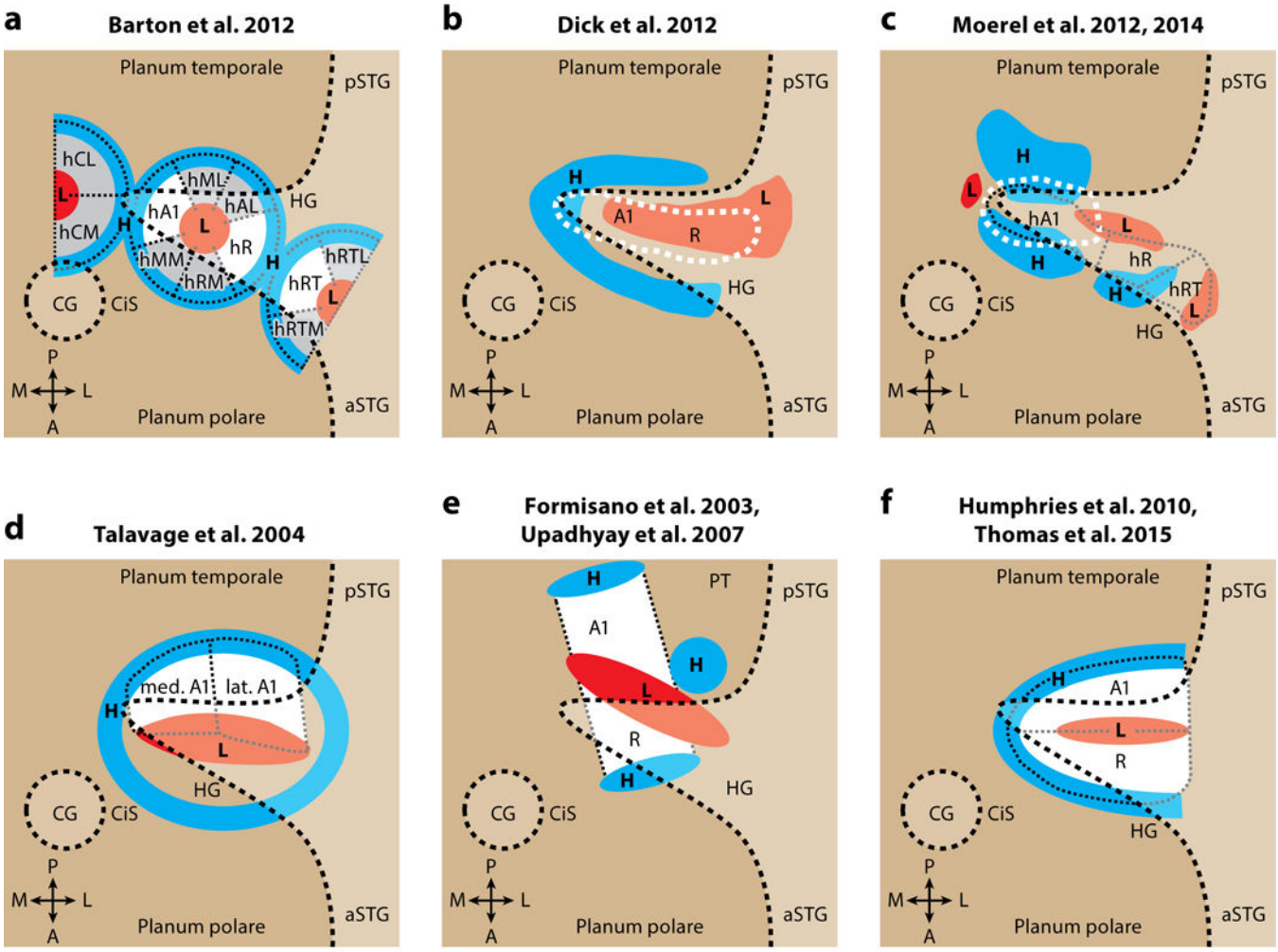

Brewer AA, Barton B. 2016.
Annu. Rev. Neurosci. 39:385–407

Figure 4.

Model comparisons: tonotopy overlapping HG. Models of human tonotopic organization are overlaid on flattened sections of cortex and are representations of the original models cited above each figure panel, modified for comparative consistency here. Darker beige background indicates sulci or the plane of the lateral sulcus, whereas lighter beige overlay indicates gyri. All panels are oriented along the same global anatomical axes (see inset legends; M, medial; L, lateral; A, anterior; P, posterior). (*a*) Model of human core (*white*) and belt (*gray*) cortical field maps overlaid with high (H, *blue*) and low (L, *red*) tonotopic representations. Auditory field maps were defined using two orthogonal dimensions: tonotopy and periodotopy, using only individual-subject data. (*b*) Model of tonotopic representations along HG from group-averaged and individual-subject tonotopic measurements. A region of central core as defined by group-averaged myelin-mapping data is marked by the white dotted line. Human A1 and R were predicted to be along HG within the bounds of these two measurements. (*c*) Model of tonotopic representations along HG

from group-averaged and individual-subject tonotopic measurements. A region of central core as defined by group-averaged and individual-subject myelin-mapping data is again marked by the white dotted line. hA1 was predicted to be along the medial tip of HG within the bounds of these two measurements. hR and hRT were approximated along HG using the tonotopic measurements only. (*d*) Model of tonotopic representations along HG from individual-subject measurements of frequency-dependent (tonotopic) responses. The proposed correspondence between one section of frequency responses along HG and the possible location ofhuman A1 is shown in the schematic. (*e*) Model of tonotopic representations along and near HG from group-averaged tonotopic measurements. Note the differences in proposed area size between this model and the other examples: The regions defined as human A1 and R using only group-averaged tonotopic measurements extend from HG well into PT. (*f*) Model of tonotopic representations along HG from tonotopic measurements. In Humphries et al. (2010), both group-averaged and individual-subject data were presented, but the cortical area model was created by overlaying the macaque core and belt model upon the group-averaged human tonotopic data. In Thomas et al. (2015), individual-subject tonotopic data were combined with bandwidth measurements to produce a very similar model for the locations of hA1 and hR. Abbreviations: aSTG, anterior superior temporal gyrus; CG, circular gyrus; CiS, circular sulcus; h, human; HG, Heschl's gyrus; lat. A1, lateral first auditory area; med. A1, medial first auditory area; pSTG, posterior superior temporal gyrus; PT, planum temporale. Other details are as in Figure 3.

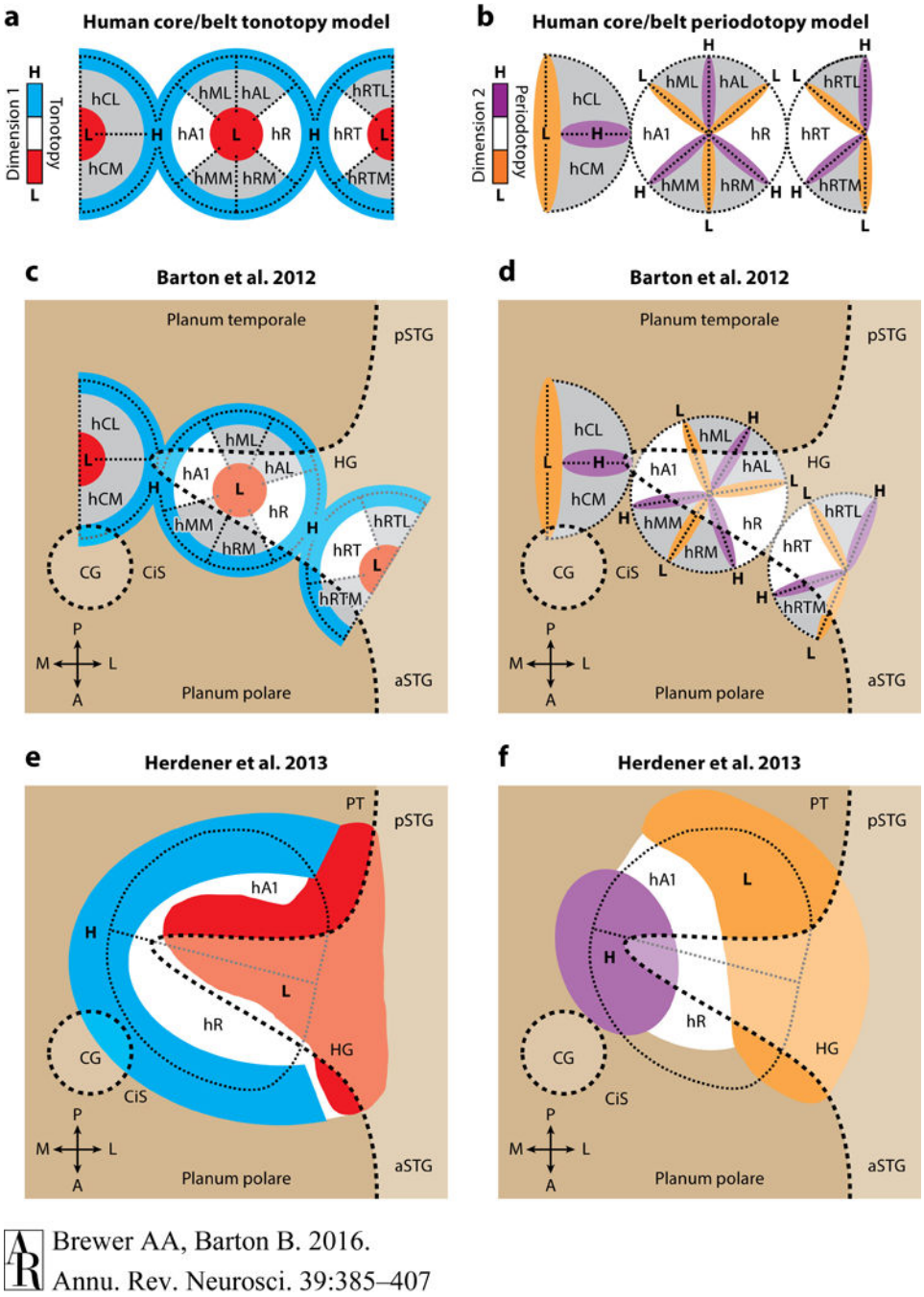

Brewer AA, Barton B. 2016.
Annu. Rev. Neurosci. 39:385–407

Figure 5.

Model comparisons: orthogonal gradients overlapping HG. (*a*) Schematic diagram shows tonotopic representations overlaid along the core (*white*) and belt (*gray*) CFMs of human auditory cortex, as defined by Barton et al. (2012). L and H denote low (*red*) or high (*blue*) tonotopic responses, respectively. (*b*) Schematic diagram shows periodotopic representations overlaid along the core (*white*) and belt (*gray*) CFMs of human auditory cortex, as defined by Barton et al. (2012). L and H here refer to low (*orange*) or high (*purple*) periodotopic responses, respectively. (*c*—*f*) Models of human AFM organization are overlaid on flattened

sections of cortex and are representations of the original models cited above each figure panel, modified for comparative consistency here. Darker beige background indicates sulci or the plane of the lateral sulcus, whereas lighter beige overlay indicates gyri. All panels are oriented along the same global anatomical axes (see inset legends; M, medial; L, lateral; A, anterior; P, posterior). (*c*) The first model of human AFM organization is shown with representations of high (H, *blue*) and low (L, *red*) tonotopic responses denoted along the borders of the 11 AFMs. Data were based on individual-subject measurements. (*d*) The same model of human AFM organization is shown now with high (H, *purple*) and low (L, *orange*) periodotopic responses overlaid on the borders of the same 11 AFMs. Data were again based on individual-subject measurements. (*e*) A model of tonotopic representations surrounding HG is shown with the estimated locations of hA1 and hR. Data were based on group-averaged measurements. (*f*) A model of periodotopic representations surrounding HG and corresponding to the tonotopic model in panel *e* is now shown, again overlaid with the estimated locations of hA1 and hR. Data were again based on group-averaged measurements. Abbreviations: AFM, auditory field map; aSTG, anterior superior temporal gyrus; CFM, cortical field map; CG, circular gyrus; CiS, circular sulcus; HG, Heschl's gyrus; pSTG, posterior superior temporal gyrus; PT, planum temporale. Other details are as in Figure 3.

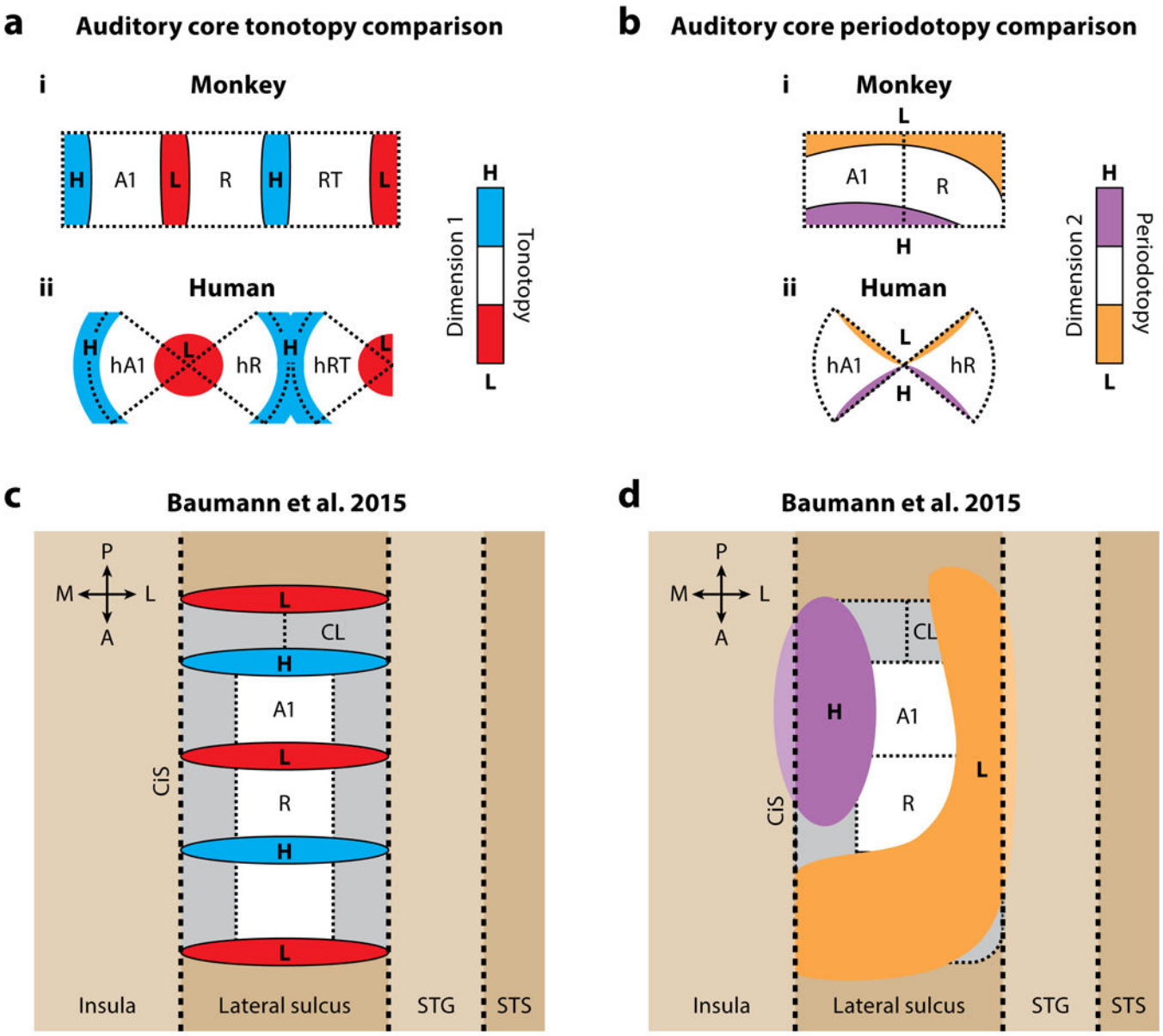

Brewer AA, Barton B. 2016.
Annu. Rev. Neurosci. 39:385–407

Figure 6.

Orthogonal gradients in macaque primary auditory cortex. (*a,b*) Diagrams show comparisons of macaque (i) and human (ii) tonotopic (*a*) and periodotopic (*b*) representations in core AFMs. Only core is shown to highlight the similarity between the species in these maps. (*c,d*) AFMs defined by orthogonal tonotopy (*C*) and periodotopy (*d*) measurements in macaque auditory cortex are shown overlaid on flattened sections of cortex and modified for comparative consistency here. The orthogonal measurements were primarily able to identify macaque AFMs A1, R, and CL. Darker beige background indicates sulci or the plane of the lateral sulcus, whereas lighter beige overlay indicates gyri. All panels are oriented along the

same global anatomical axes (see inset legends; M, medial; L, lateral; A, anterior; P, posterior). Abbreviations: A1, first auditory area; AFMs, auditory field maps; CL, caudal lateral area; h, human; R, rostral area; STG, superior temporal gyrus; STS, superior temporal sulcus. Other details are as in Figure 3.